available at www.sciencedirect.com

ScienceDirect

journal homepage: www.elsevier.com/locate/chnjc

Article

HZSM-35 zeolite catalyzed aldol condensation reaction to prepare acrylic acid and its ester: Effect of its acidic property

Zhanling Ma [a,b,c], Xiangang Ma [a], Youming Ni [a], Hongchao Liu [a], Wenliang Zhu [a,#], Xinwen Guo [b], Zhongmin Liu [a,*]

[a] *National Engineering Laboratory for Methanol to Olefins, Dalian Institute of Chemical Physics, Chinese Academy of Sciences, Dalian 116023, Liaoning, China*

[b] *State Key Laboratory of Fine Chemicals, PSU-DUT Joint center for Energy Research, School of Chemical Engineering, Dalian University of Technology, Dalian 116024, Liaoning, China*

[c] *University of Chinese Academy of Sciences, Beijing 100049, Beijing, China*

ARTICLE INFO

Article history:
Received 21 June 2018
Accepted 16 July 2018
Published 5 November 2018

Keywords:
Aldol condensation
Methyl acetate
ZSM-35 zeolite
Brönsted acid
Acrylic acid

ABSTRACT

Acrylic acid (AA) and its ester, methyl acrylate (MA), were produced by a green one-step aldol condensation reaction of dimethoxymethane and methyl acetate. The reaction was conducted over ZSM-35 zeolites with different concentrations of Brönsted acid, which were prepared by the sodium ion-exchange process with H-form zeolite. The acidic property of HZSM-35 was studied in detail through infrared experiments. About 51% of all bridging OH groups were distributed in cages, while 23% and 26%, respectively, were distributed in 10- and 8-ring channels. The catalytic performance was enhanced by a high concentration of Brönsted acid, indicating that Brönsted acid is an active site for the aldol condensation reaction. The ZSM-35 zeolite possessing a concentration of Brönsted acid as high as 0.049 mmol/g demonstrated excellent performance with a MA+AA selectivity of up to 73%.

1. Introduction

Acrylic acid (AA) and methyl acrylate (MA), the two extremely important industrial chemicals, are widely applied in the production of paintings, coatings, carbon fibers, and adhesives. They are mostly produced by a two-step oxidation reaction of propylene [1–3]. This route of oxidation by air/oxygen incurs a risk of over-oxidation of propylene and the desired products, which limits their widespread application on a large scale. Therefore, a novel and green route for MA and AA synthesis is highly demanded. Recently, the route to produce MA and AA through a one-step aldol condensation reaction of formaldehyde (FA) and methyl acetate (MAc) has been attracting substantial interest from both academic and industrial communities because of its simplicity and common feedstocks that can be derived readily from natural gas, coal, and biomass [4,5].

Aldol condensation reaction, which is catalyzed by acid/base catalysts, can readily occur over either an acid (or a base) or an acid-base bifunctional catalyst. Previous studies have mainly focused on aldol condensation catalyzed by a variety of cesium supported with SiO_2 or SBA-15 [6–9], by acid–base bifunctional catalysts such as V_2O_5-P_2O_5 binary or V_2O_5-P_2O_5-SiO_2 ternary systems [10–13], or by alkali metal oxide-supported acidic catalysts [14–16]. However, there are limited experimental data available for evaluating the performance of solid acid catalysts in the aldol condensation reaction

* Corresponding author. Tel: +86-411-84379998; Fax: +86-411-84379038; E-mail: liuzm@dicp.ac.cn
# Corresponding author. Tel: +86-411-84379418; Fax: +86-411-84379038; E-mail: wlzhu@dicp.ac.cn
DOI: 10.1016/S1872-2067(18)63145-6 | http://www.sciencedirect.com/science/journal/18722067 | Chin. J. Catal., Vol. 39, No. 11, November 2018

in the gaseous phase. Zeolite catalysts, as a type of solid catalysts being comprehensively utilized for more than 40% industrial processes in petroleum and petrochemical fields [17], show significant potential in aldol condensation. In our previous study [18], several types of zeolites, including HY, Hß, HMOR, HZSM-5, and HZSM-35, were first used as aldol condensation catalysts for synthesizing MA and AA with high activity, which suggested that zeolite is a catalyst candidate for the aldol condensation reaction of FA and MAc.

It is well known that two types of acids, Brönsted and Lewis acids, exist in zeolites, especially in silica-alumina zeolites. However, the issue of whether the aldol condensation reaction occurs over Lewis acid sites, Brönsted acid sites, or both has not been resolved yet. Jeong et al. [19] reported the results from in situ Fourier-transform infrared spectroscopy (FT-IR) studies of aldol condensation reactions of aldehydes with $AlPO_4$ zeolite as a catalyst. They found that Lewis acid was the active site for the aldol condensation reaction due to the lack of a bridging hydroxyl group in the $AlPO_4$ zeolite catalyst. Panov et al. [20] conducted aldol condensation reactions over nanosized amorphous alumina catalysts containing different amounts of Lewis acid sites and found that the rate of aldol condensation reaction of acetone decreased with the loss of Lewis acid sites. Dumitriu et al. [21] synthesized a series of MFI zeolites by isomorphous substitution of Me^{3+} for silicon and evaluated them in aldol condensation reactions of acetaldehyde and formaldehyde. They found that both Brönsted and Lewis acids were involved in the reaction and that a higher Lewis acid concentration favored a better selectivity for MFI zeolite catalysts. However, Kikhtyanin et al. [22] proved that solid catalysts with exclusive Lewis acid sites possessed substantially lower activity in the aldol condensation of furfural and acetone with MOFs as acidic catalysts, and suggested that Brönsted acid contributed more to the aldol condensation reaction than Lewis acid. Kikhtyanin et al. [23] also reported that two HBEA samples with the same Brönsted acid concentration but different Lewis acid concentrations exhibited approximately the same activity. They believed that the aldol condensation reaction proceeded with the participation of Brönsted acid rather than Lewis acid.

In our previous studies [16,18], HZSM-35 zeolite was found to perform very well in the aldol condensation reaction of MAc and formaldehyde, and its acid site was found to be indispensable for triggering the reaction. To the best of our knowledge, no information is available yet on the effect of acidic properties of zeolites on the aldol condensation of formaldehyde and MAc to prepare MA and AA. Therefore, here, we study in detail the acidic property of HZSM-35 and prepare ZSM-35 with different concentrations of Brönsted acid through the sodium ion-exchange process without altering the concentration of Lewis acid. We then evaluate the catalytic performance of ZSM-35 zeolites for the aldol condensation reaction of formaldehyde and MAc.

2. Experimental

2.1. Catalyst preparation

The regents used included dimethoxymethane (DMM) (AR, 98%, Alfa Aesar (China) Chemicals Co., Ltd.) and MAc (AR, 98%, Sinopharm Chemical Reagent Co., Ltd., China). Na-ZSM-35 (SiO_2/Al_2O_3 = 79) was purchased from Shanghai Novel Chemical Technology Co., Ltd., China. Zeolite was calcinated at 823 K in air for at least 5 h to remove the retained organic template, and then converted into an H-form zeolite before use by conducting ion exchange thrice at 353 K for 6 h in 1 mol/L NH_4NO_3 solution, followed by washing with deionized water, drying at 373 K overnight, and calcination at 823 K for 4 h. To obtain zeolites with different sodium ion weight percentages, the H-form zeolite powder began to be exchanged with $NaNO_3$ solution (0.1 mol/L) at 323 K with a solid-to-liquid ratio of 1/20 for different times. The filter cake was dried at 373 K for 12 h. At last, we obtained zeolite with different sodium ion-exchange degrees. The sample was indicated as Na-Z-x, where x indicates the molar ratio of sodium element to aluminum element in the zeolite characterized by X-ray fluorescence (XRF) results.

2.2. Catalyst characterization

FT-IR spectroscopy was conducted at a spectral resolution of 4 cm^{-1} on a Bruker Tensor 27 FT-IR spectrophotometer equipped with a mercury-cadmium-telluride detector, which was sensitive to –OH group vibration. The sample was pressed into a self-supporting disk with a diameter of 13 mm. Then, the disk was put into a quartz cell, which was connected to a vacuum system and sealed with CaF_2 windows and then heated to 723 K for at least 4 h to remove the retained water before collecting the spectra. The pyridine or acetonitrile adsorption was performed by exposing the preheated disk to its vapor. The semi-quantitative analysis of the concentration of Brönsted or Lewis acid is shown as below [24]:

$$C(\text{pyridine on B sites}) = 1.88\ IA(B)\ R^2/W$$

$$C(\text{pyridine on L sites}) = 1.42\ IA(L)\ R^2/W$$

C = concentration (mmol/g catalyst)

IA(B, L) = integrated absorbance of B or L band (cm^{-1})

R = radius of catalyst disk (cm^{-1})

W = weight of disk (mg)

The solid-state NMR experiments were carried out on a Bruker AvanceIII 600 spectrometer equipped with a 14.1 T wide-bore magnet. The bulk acidity of zeolite was determined by temperature-programmed desorption of ammonia (NH_3-TPD) on a Micromeritics AutoChem 2920 instrument. The sample (0.20 g) was loaded in a U-shaped microreactor and preheated at 823 K for 0.5 h under helium atmosphere. After cooling to 373 K, the sample was saturated with ammonia, followed by purging with helium to remove the physically adsorbed ammonia molecule. Ammonia desorption was conducted in helium flow (30 mL/min) by heating from 373 to 923 K at a rate of 10 K/min and measured by a thermal conductivity detector.

The crystallinity of the samples was characterized by a PANalytical X'Pert PRO X-ray diffraction (XRD) meter with Cu-K_α radiation (λ = 1.51059 Å) at 40 kV and 40 mA. The chemical composition of zeolite was determined by Philips Magix-601 XRF. Nitrogen adsorption-desorption isotherms

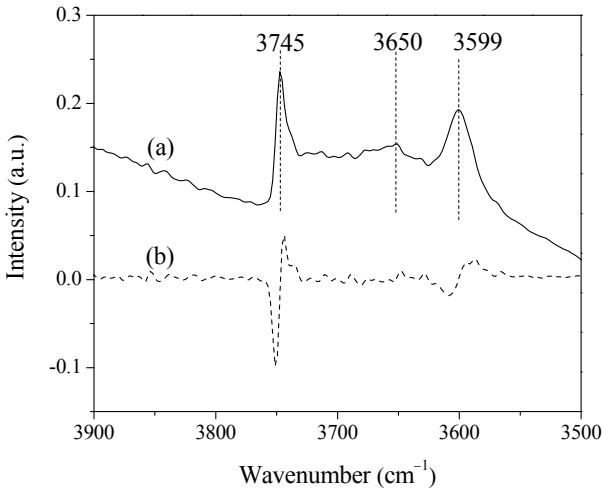

Fig. 1. OH regions of (a) the IR spectrum of HZSM-35 zeolite measured at 298 K after evacuation at 723 K and (b) its first derivative.

were obtained on a Micrometrics ASAP 2020 system at 77 K.

2.3. Catalytic test

Aldol condensation of formaldehyde with MAc was carried out at 623 K with 0.5 g zeolite (20–40 mesh) in a fixed bed. Here, DMM was applied as the source of formaldehyde. The system pressure was set at 3 MPa. DMM and MAc precursors in two separated stainless-steel tubes held at 293 K were bubbled into the reaction tube by 30 mL/min N_2 flow, respectively. The products were analyzed using an online gas chromatograph equipped with a flame ionization detector connected to an FFAP capillary column. The yield of MA and AA was defined as $moles_{MA+AA}/moles_{MAc\ fed}$ and S_{MA+AA} was calculated using the $moles_{MA+AA}/moles_{MAc}$ consumed.

3. Results and discussion

3.1. Acidity of HZSM-35 zeolite

FT-IR spectroscopy is applied to characterize the acid property of HZSM-35 zeolite, as shown in Fig. 1. The spectrum of HZSM-35 zeolite in Fig. 1(a) consists of two distinct bands at 3745 cm^{-1} due to the terminal silanol groups and at 3599 cm^{-1} due to the bridging hydroxyl groups (Brönsted acid sites) [25–27]. The relatively high intensity of silanol groups at 3745 cm^{-1} shows that HZSM-35 zeolite is high-siliceous, which agrees with the XRF result indicating a high SiO_2/Al_2O_3 ratio of 79. In addition, a broad band around 3650 cm^{-1} is assigned to OH groups adjacent to extra-framework aluminum species. A close examination reveals that hydroxyl IR bands are asymmetric, which is particularly evident from the first derivative of the spectrum. The asymmetry at 3745 cm^{-1} can be attributed to the presence of terminal silanol groups and to their hydrogen bonding interaction, while that at 3599 cm^{-1} is associated with the Brönsted acidic bridging hydroxyl moieties vibrating in channels or cages of different sizes [28].

The ^{29}Si MAS NMR spectrum of HZSM-35 zeolite in Fig. 2(a) shows three signals at –105.7, –112.1, and –116.6 ppm, which are assigned to Si(1Al) T_A, the superposition of Si(1Al) T_A and Si(0Al) T_B, and Si(0Al) T_B, respectively [29–31]. The high ratio of Si(0Al) and Si(1Al) contributions indicates the prevalence of the Si–O–Si bond in the absence of neighboring Al. Fig. 2(b) shows the ^{27}Al MAS NMR spectrum of HZSM-35 zeolite used here, where the signal at 54.5 ppm is attributed to tetrahedrally coordinated framework aluminum atoms. The signal at 0 ppm indicates the presence of a few octahedrally coordinated extra-framework aluminum species, acting as Lewis acid sites, which is consistent with the FT-IR observation in Fig. 1.

Fig. 3 shows the deconstruction of the bridging OH band in the IR spectra of HZSM-35 according to Zholobenko et al. [28]. A good fit is obtained by decomposition based on three peaks. The 3610 cm^{-1} band can be attributed to Si–O(H)–Al groups in 10-member rings, amounting to 23% of Si–O(H)–Al groups. The intense band at 3600 cm^{-1} can be assigned to the bridging hydroxyl groups in cages at the intersection of 8- and 6-ring channels, amounting to 51% of the bridging hydroxyl groups. The band at 3588 cm^{-1} can be attributed to Si–O(H)–Al groups in 8-member rings. Such an assignment coincides with the republished work. For instance, the initially observed band in bridging OH groups at about 3610 cm^{-1} in H-mordenite is deconvoluted into two component bands, one at a higher frequency of 3612 cm^{-1} and another at a lower frequency of 3585

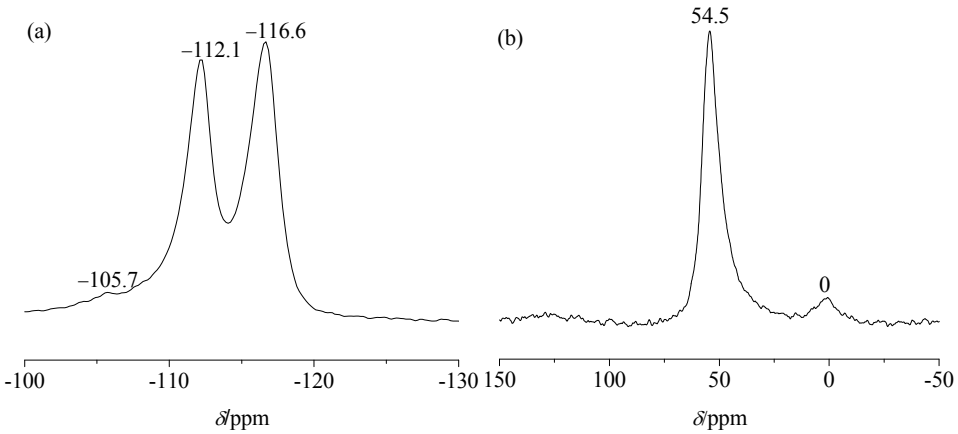

Fig. 2. (a) ^{29}Si and (b) ^{27}Al MAS NMR spectra of HZSM-35 zeolite.

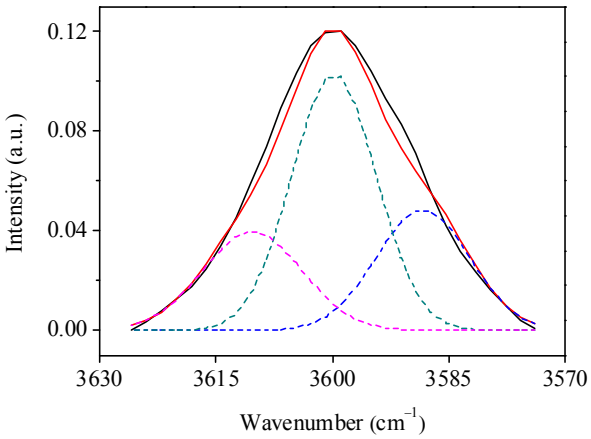

Fig. 3. Deconstruction of the bridging OH band in the IR spectrum of HZSM-35. (–, experimental spectrum; ····, computed spectrum; - - -, single components).

cm^{-1}, which are assigned to OH groups in 12- and 8-ring channels, respectively [32–35]. The low-frequency-component IR band is attributed to Brönsted acid sites in a small channel, while the high-frequency one is attributed to those in a large ring, such as 8- or 10-rings [36–38].

Fig. 4(a) describes that pyridine adsorption in HZSM-35 zeolite takes place only on a part of the bridging OH groups in vacuum at room temperature with a small decrease in intensity at 3599 cm^{-1}, while the smaller acetonitrile molecule interacts with all bridging OH groups under the same conditions as the intensity at 3599 cm^{-1} immediately decreases. This in turn proves the heterogeneous distribution of internal bridging OH groups in HZSM-35 zeolite. The accessibility of the internal Bronsted acidic bridging OH groups for pyridine molecules is studied with respect to temperature, as shown in Fig. 4(b). The intensity of the IR band at 3599 cm^{-1} characteristic for strong acidic bridging OH groups clearly decreases after adsorption at 373 K. With an increase in the temperature of pyridine adsorption, more adsorption of pyridine on bridging OH groups of HZSM-35 zeolite takes place as follows from a decline in the intensity of the band at 3599 cm^{-1}. This means that the internal bridging OH groups are accessible to large pyridine molecules at high temperature [39,40]. The existence of two bands at 3597 and 3589 cm^{-1} is revealed after pyridine adsorption at different temperatures. The bridging OH groups located in the smaller channels are not so easily accessible for large pyridine molecules as those in the main channels. It seems reasonable to assign these two bands at 3597 and 3589 cm^{-1} to the bridging OH groups located in cages and 8-ring channels, respectively, which supports our decomposition results shown in Fig. 3.

3.2. Effect of the concentration of Brönsted acid on catalytic performance

Zeolites, which are crystalline alumino-silicate microporous materials, possess interesting intrinsic acidic features, such as Lewis and Brönsted acid sites. Brönsted acid sites exist as bridging OH groups to Al and Si atoms, and their protons can be exchanged with other metal cations. Herein, we prepare ZSM-35 zeolites with varying concentrations of Brönsted acid through the sodium ion-exchange process. The crystalline structure and textural property are not affected by the exchange process, as shown in Fig. S1 and S2.

The IR characterization is used to clarify the change in the acidic properties of zeolites after the treatment. The intensity of the bridging OH groups at 3599 cm^{-1} suffers a significant decrease after sodium ion exchange, as illustrated in Fig. 5(a), which indicates that the Brönsted acidic proton of HZSM-35 zeolite is substituted by Na^+. A higher exchange degree leads to a lower intensity of the Brönsted acid hydroxyl groups. In HZSM-35 zeolite, the IR band of PyH^+ appears at 1545 cm^{-1} after adsorption of pyridine at 623 K for 30 min with the band of pyridine adsorbed on typical Lewis acid sites at 1445 cm^{-1} (Fig. 5(b)) [41,42]. The Lewis acid sites in HZSM-35 are assigned to the extra-framework aluminum species. The intensity of the band at 1545 cm^{-1} drops significantly with the pretreatment of the sodium ion-exchange process, which indicates a decrease in the concentration of Brönsted acid in ZSM-35 zeolite. As shown in Table 1, the concentration of the Brönsted acid in HZSM-35 zeolite, obtained by the integration of the band at 1545 cm^{-1}, is 0.049 mmol/g, which decreases to 0.037 mmol/g in Na-Z-25 zeolite and even falls to 0.011 mmol/g in Na-Z-49

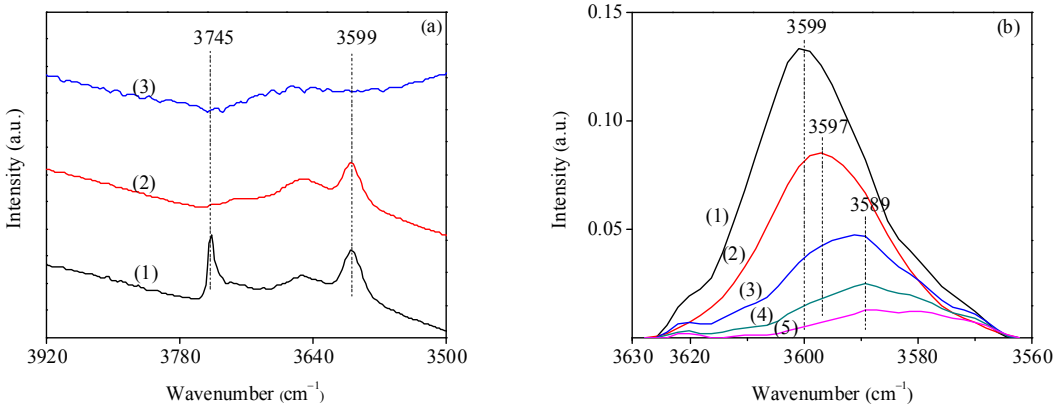

Fig. 4. (a) FT-IR spectra of OH groups of HZSM-35 at 298 K after evacuation at 723 K (1), after adsorption of pyridine at 298 K (2), and after adsorption of acetonitrile at 298 K (3). (b) FT-IR spectra of the bridging OH groups of HZSM-35 (1), after adsorption of pyridine at 373 K (2), 523 K (3), 623 K (4), and 723 K (5).

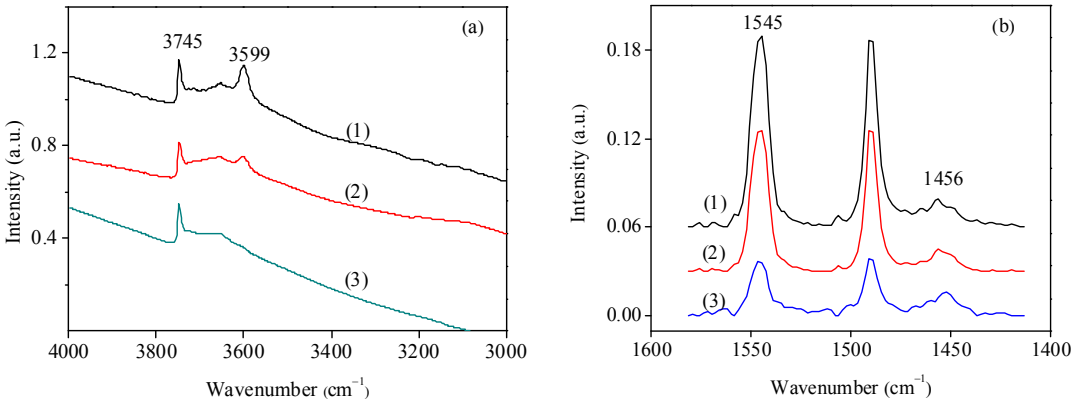

Fig. 5. (a) FT-IR characterization of OH regions of HZSM-35 zeolite (1) and Na-Z-25 (2) and Na-Z-49 (3) at 298 K after evacuation at 723 K; (b) Pyridine adsorption at 623 K for 30 min and desorption at the same time of HZSM-35 zeolite (1) and Na-Z-25 (2) and Na-Z-49 (3).

zeolite. The concentration of the Lewis acid remains constant at 0.004 mmol/g.

The effect of this sodium ion-exchange process on the bulk acidity of zeolite is studied using NH_3-TPD, as described in Fig. 6. Two ammonia desorption peaks are found at 465 and 709 K in HZSM-35 (Fig. 6(a)), which shows that two types of acid sites, including the weak and the strong ones, exist in the sample. The intensity of the latter peak suffers a decrease in Na-Z-25 zeolite, and even becomes a broad tail in Na-Z-49 zeolite. Note that the strength of the strong acid does not change in the sodium ion-exchange process for its peak temperature being maintained constant at 709 K. Taken together, the above results show that a large amount of strong Brönsted acid is substituted by the sodium ion, resulting in a loss of strong acidity in HZSM-35 zeolite.

The performance of ZSM-35 zeolites with different concentrations of Brönsted acid in the aldol condensation reaction of FA and MAc is evaluated in a continuous-flow fixed-bed reaction tube as illustrated in Fig. 7. Herein, dimethoxymethane (DMM) is employed as the source of FA. The mass spectrum detection result shown in Fig. S3 substantiates the facile decomposition of DMM to attain FA with 100% conversion in Fig. S4 over all ZSM-35 zeolites. MAc conversion changes slightly over all ZSM-35 zeolites, as shown in Fig. S4. However, the yield and S_{MA+AA} are remarkably enhanced parallel to the increase in the concentration of Brönsted acid in zeolites. Here, note that AA is mainly derived from the hydrolysis of MA and the ratio of MA to AA varies from 1 to 4. Given that the concentration of Lewis acid remains constant at 0.004 mmol/g for all zeolites, it is suggested that Brönsted acid is an active site for the aldol condensation reaction of DMM and MAc. The rate-determined step of aldol condensation reaction in the gaseous phase is reported to be the keto-enol tautomerization of MAc. The enol form of MAc reacts with FA to produce MA and AA. With a high concentration of Brönsted acid, the keto-enol tautomerization equilibrium might shift significantly to an enol counterpart, which consecutively reacts with FA to give a high S_{MA+AA} and yield.

The deposited coke amounts of deactivated ZSM-35 zeolites with different concentrations of Brönsted acid after aldol condensation reaction for 6 h are determined by TGA characterization. As shown in Fig. 8, the TGA results show that the amounts of deposited coke in HZSM-35, Na-Z-25, and Na-Z-49 are 8%, 5.5%, and 2.5%, respectively, among which HZSM-35 zeolite has the highest coke amount. Considering the difference in Brönsted acid concentration of the three catalysts, the lowest amount of coke within Na-Z-49 zeolite is ascribed to its low concentration of Brönsted acid. From the first derivative curve of TGA, the consumption temperatures of coke species within HZSM-35, Na-Z-25, and Na-Z-49 zeolites are 904, 860, and 819 K, respectively. HZSM-35 zeolite has the hardest coke species, which mainly consists of benzene, naphthalene, phenanthrene, and their methyl-substituted derivatives, as described in Fig. S5. The unsaturated product, MA and AA, might continue to perform the Diels-Alder ring-closing reaction on Brönsted acid sites to form aromatic species. On the other hand, the methanol-to-hydrocarbons reaction is unavoidable at such high reac-

Table 1
Acidic properties of ZSM-35 zeolites after sodium ion-exchange treatment.

Sample	SiO_2/Al_2O_3	B* (mmol/g)	L* (mmol/g)
HZSM-35	79	0.049	0.004
Na-Z-25	79	0.037	0.004
Na-Z-49	82	0.011	0.004

*Calculated through integration of IR peak.

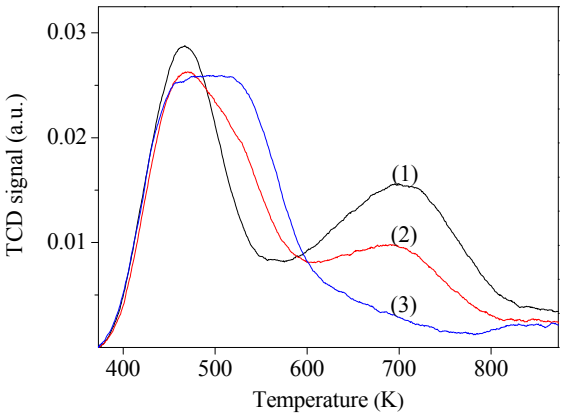

Fig. 6. NH_3-TPD curves of HZSM-35 (1), Na-Z-25 (2), and Na-Z-49 (3).

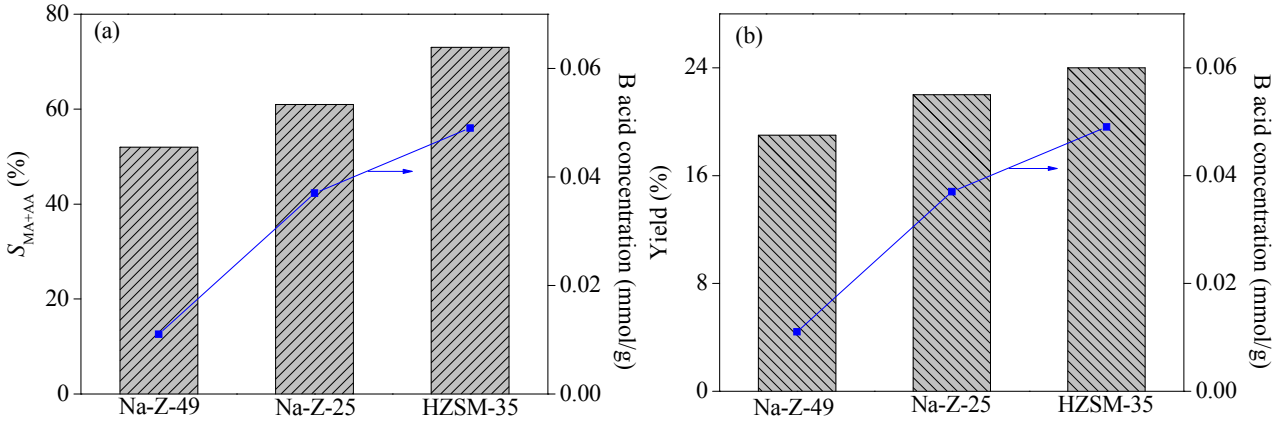

Fig. 7. Effect of the concentration of Brönsted acid of ZSM-35 zeolite on S_{MA+AA} (a) and yield (b). Reaction conditions: TOS = 150 min, 3 MPa, 623 K; the saturated vapor pressures of DMM and MAc were 43.3 and 23.0 kPa, respectively; n_{DMM}/n_{MAc} = 2/1; SiO_2/Al_2O_3 = 79; and the total gas flow rate was 60 mL/min.

tion temperature of 623 K in the presence of a strong Brönsted acid and an amount of C_1–C_5 hydrocarbon product is detected in the initial period of the first 60 min. This reaction might also cause the deactivation of zeolites.

4. Conclusions

The distribution of Brönsted acid in HZSM-35 zeolite was systemically studied by IR experiments, and 51% of the total Brönsted acid was found to be located in the cage, while 23% and 26% were distributed in 10- and 8-ring channels, respectively. Brönsted acid was an active site for aldol condensation reaction of DMM and MAc for producing MA and AA. A high concentration of Brönsted acid was beneficial to the selectivity and yield of MA and AA. This study provided more information about the acid-catalyzed aldol condensation reaction. Moreover, the accurate position of the site of aldol condensation reaction in the framework, whether in a cage or in a 10- or 8-ring channel, as well as the effect of Lewis acid sites, need to be studied further.

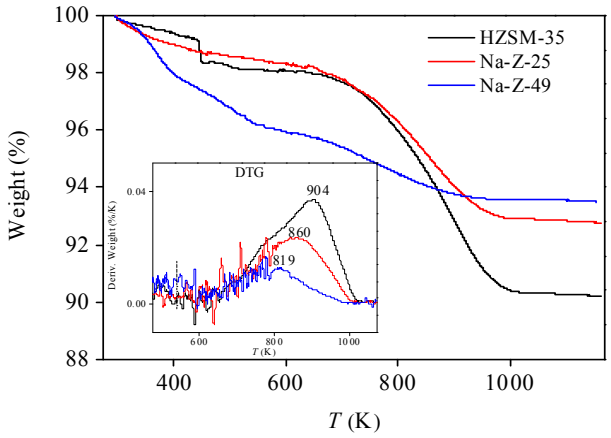

Fig. 8. TGA curves and their derivates (the inset graph) of deactivated HZSM-35, Na-Z-25, and Na-Z-49 zeolites obtained after the aldol condensation reaction of DMM and MAc at 623 K.

References

[1] M. M. Bettahar, G. Costentin, L. Savary, J. C. Lavalley, *Appl. Catal. A,* **1996**, 145, 1–48.

[2] W. Fang, Q. J. Ge, J. F. Yu, H. Y. Xu, *Ind. Eng. Chem. Res.*, **2011**, 50, 1962–1967.

[3] W. E. Campbell, E. L. McDaniel, W. H. Reece, J. E. Williams, H. S. Young, *Ind. Eng. Chem. Prod. Res. Develop.*, **1970**, 9, 325–334.

[4] J. F. Vitcha, V. A. Sims, *Ind. Eng. Chem. Prod. Res. Develop.*, **1966**, 5, 50–53.

[5] L. H. Zhao, J. Yan, L. C. Wei, Y. L. Jiang, *Mod. Chem. Ind.*, **2015**, 35, 44–49.

[6] B. Harris, *Ingenia*, **2010**, 45, 18–23.

[7] Y. N. Wang, X. W. Lang, G. Q. Zhao, H. H. Chen, Y. W. Fan, L. Q. Yu, X. X. Ma, Z. R. Zhu, *RSC Adv.*, **2015**, 5, 32826–32834.

[8] J. B. Yan, C. L. Zhang, C. L. Ning, Y. Tang, Y. Zhang, L. L. Chen, S. Gao, Z. L. Wang, W. X. Zhang, *J. Ind. Eng. Chem.*, **2015**, 25, 344–351.

[9] T. He, Y. X. Qu, J. D. Wang, *Ind. Eng. Chem. Res.*, **2018**, 57, 2773–2786.

[10] H. Zhao, C. C. Zuo, D. Yang, C. S. Li, S. J. Zhang, *Ind. Eng. Chem. Res.*, **2016**, 55, 12693–12702.

[11] D. Yang, C. Sararuk, K. Suzuki, Z. X. Li, C. S. Li, *Chem. Eng. J.*, **2016**, 300, 160–168.

[12] J. Hu, Z. P. Lu, H. B. Yin, W. P. Xue, A. L. Wang, L. Q. Shen, S. X. Liu, *J. Ind. Eng. Chem.*, **2016**, 40, 145–151.

[13] D. Yang, D. Li, H. Y. Yao, G. L. Zhang, T. T. Jiao, Z. X. Li, C. S. Li, S. J. Zhang, *Ind. Eng. Chem. Res.*, **2015**, 54, 6865–6873.

[14] C. Sararuk, D. Yang, G. L. Zhang, C. S. Li, S. J. Zhang, *J. Ind. Eng. Chem.*, **2017**, 46, 342–349.

[15] A. L. Wang, J. Hu, H. B. Yin, Z. P. Lu, W. P. Xue, L. Q. Shen, S. X. Liu, *RSC Adv.*, **2017**, 7, 48475–48485.

[16] Z. L. Ma, X. G. Ma, H. C. Liu, W. L. Zhu, X. W. Guo, Z. M. Liu, *Chin. J. Catal.*, **2018**, 39, 1129–1137.

[17] K. Tanabe, W. F. Hölderich, *Appl. Catal. A*, **1999**, 181, 399–434.

[18] Z. L. Ma, X. G. Ma, H. C. Liu, Y. L. He, W. L. Zhu, X. W. Guo, Z. M. Liu, *Chem. Commun.*, **2017**, 53, 9071–9074.

[19] M. S. Jeong, H. Rrei, *J. Mol. Catal. A*, **2000**, 156, 245–253.

[20] A. G. Panov, J. J. Fripiat, *Catal. Lett.*, **1999**, 57, 25–32.

[21] E. Dumitriu, V. Hulea, I. Fechete, A. Auroux, J. F. Lacaze, C. Guimon, *Microporous Mesoporous Mater.*, **2001**, 43, 341–359.

[22] O. Kikhtyanin, D. Kubička, J. Čejka, *Catal. Today*, **2015**, 243, 158–162.

Graphical Abstract

Chin. J. Catal., 2018, 39: 1762–1769 doi: 10.1016/S1872-2067(18)63145-6

HZSM-35 zeolite catalyzed aldol condensation reaction to prepare acrylic acid and its ester: Effect of its acidic property

Zhanling Ma, Xiangang Ma, Youming Ni, Hongchao Liu, Wenliang Zhu *, Xinwen Guo, Zhongmin Liu *
Dalian Institute of Chemical Physics, Chinese Academy of Sciences;
Dalian University of Technology;
University of Chinese Academy of Sciences

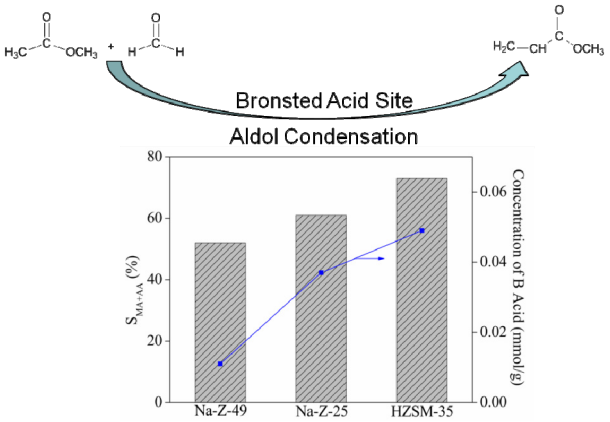

Brönsted acid was an active site for aldol condensation reaction of DMM and MAc to produce MA and AA. The selectivity of MA and AA increased with the concentration of Brönsted acid.

[23] O. Kikhtyanin, V. Kelbichová, D. Vitvarová, M. Kubů, D. Kubička, *Catal. Today*, **2014**, 227, 154–162.
[24] C. A. Emeis, *J. Catal.*, **1993**, 141, 347–354.
[25] M. Trombetta, G. Busca, S. Rossini, V. Piccoli, U. Cornaro, A. Guercio, R. Catani, R. J. Willey, *J. Catal.*, **1998**, 179, 581–596.
[26] Y. S. Jin, A. Auroux, J. C. Vedrine, *Appl. Catal.*, **1988**, 37, 1–19.
[27] P. Cañizares, A. Carrero, *Catal. Lett.*, **2000**, 64, 239–246.
[28] V. L. Zholobenko, D. B. Lukyanov, J. Dwyer, W. J. Smith, *J. Phys. Chem. B*, **1998**, 102, 2715–2721.
[29] D. P. B. Peixoto, S. M. Cabral de Menezes, M. I. Pais da Silva, *Mater. Lett.*, **2003**, 57, 3933–3942.
[30] A. Bonilla, D. Baudouin, J. Pérez-Ramírez, *J. Catal.*, **2009**, 265, 170–180.
[31] R. Rachwalik, Z. Olejniczak, J. Jiao, J. Huang, M. Hunger, B. Sulikowski, *J. Catal.*, **2007**, 252, 161–170.
[32] F. Wakabayashi, J. Kondo, A. Wada, K. Domen, C. Hirose, *J. Phys. Chem.*, **1993**, 97, 10761–10768.
[33] V. L. Zholobenko, M. A. Makarova, J. Dwyer, *J. Phys. Chem.*, **1993**, 97, 5962–5964.
[34] S. Bordiga, C. Lamberti, F. Geobaldo, A. Zecchina, G. Turnes Palomino, C. Otero Arean, *Langmuir*, **1995**, 11, 527–533.
[35] P. A. Jacobs, W. J. Mortier, *Zeolites*, **1982**, 2, 226–230.
[36] J. E. Naber, K. P. de Jong, W. H. J. Stork, H. P. C. E. Kuipers, M. F. M. Post, *Stud. Surf. Sci. Catal.*, **1994**, 84, 2197–2219.
[37] B. Wichterlová, N. Žilkova, E. Uvarova, J. Čejka, P. Sarv, C. Paganini, J. A. Lercher, *Appl. Catal. A*, **1999**, 182, 297–308.
[38] J. Datka, M. Kawalek, K. Gora-Marek, *Appl. Catal. A*, **2003**, 243, 293–299.
[39] M. Trombetta, G. Busca, *J. Catal.*, **1999**, 187, 521–523.
[40] J. A. Z. Pieterse, S. Veefkind-Reyes, K. Seshan, L. Domokos, J. A. Lercher, *J. Catal.*, **1999**, 187, 518–520.
[41] Z. G. Zhu, H. Xu, J. G. Jiang, Y. J. Guan, P. Wu, *J. Catal.*, **2017**, 352, 1–12.
[42] Z. G. Zhu, H. Xu, J. G. Jiang, X. Liu, J. H, Ding, P. Wu, *Appl. Catal. A*, **2016**, 519, 155–164.

HZSM-35分子筛酸性质对甲缩醛和乙酸甲酯羟醛缩合反应的影响

马占玲[a,b,c], 马现刚[a], 倪友明[a], 刘红超[a], 朱文良[a,#], 郭新闻[b], 刘中民[a,*]
[a]中国科学院大连化学物理研究所甲醇制烯烃国家工程实验室, 辽宁大连116023
[b]大连理工大学化工与环境生命学部化工学院精细化工国家重点实验室, 辽宁大连116024
[c]中国科学院大学, 北京100049

摘要: 丙烯酸及其酯是重要的化工原料, 广泛应用于涂料、粘结剂、纤维等领域, 目前工业上常采用丙烯两段氧化法进行制备, 但该法以石油基原料丙烯为源头, 采用V/Mo/Bi等金属催化剂, 不符合可持续发展理念, 且存在环境污染及氧气下产物易过度氧化等问题. 如何高效、安全、大规模工业化制备丙烯酸及其酯是研究者追求的目标. 以乙酸甲酯(Mac)和甲醛为原料, 通过羟醛缩合一步制备丙烯酸及其酯是一条完全不同于丙烯氧化法的合成路径, 原料均可由煤基甲醇得到, 符合我国"富煤、贫油、少气"基本能源结构, 且该方法碳原子利用率为100%, 副产物仅为水, 属于绿色环保合成路径.

本文以甲缩醛(DMM)为甲醛源, 创新性地采用固体硅铝分子筛为酸性催化剂, 催化DMM和MAc发生羟醛缩合反应来制备丙烯酸. 硅铝分子筛具有较高的活性, 可高效地催化羟醛缩合反应, 且具有很好的再生性能, 即使催化剂寿命较短, 也可采用流化床或移动床等反应器进行工业化, 因此存在良好的工业化前景. 硅铝分子筛中常含有Brönsted酸和Lewis酸, 为试图说明羟醛缩合反应的真正活性位点, 我们以羟醛缩合反应性能最佳的HZSM-35分子筛为研究目标.

首先, 利用红外研究HZSM-35分子筛的酸性质. 发现分子筛中桥羟基提供Brönsted酸, 外骨架铝物种提供Lewis酸. 通过对桥羟基红外峰一阶求导, 发现其对称性较差, 表明Brönsted酸在HZSM-35分子筛孔道中分布不均匀. 利用红外分峰手段, 得知约51%的Brönsted酸分布于八元环和六元环交叉所形成的笼(cage)中, 约23%分布于十元环孔道, 26%分布于八元环孔道中. 同时, 利用吡啶在分子筛HZSM-35不同温度下的吸附情况验证了这一分峰结果. 其次, 利用钠离子交换方法制备不同Brönsted酸浓度的ZSM-35分子筛, 经吡啶红外表征得知, Brönsted酸浓度随钠离子交换程度增加而逐渐降低, 而Lewis酸浓度并未改变; 在羟醛缩合反应性能中, 丙烯酸及丙烯酸甲酯选择性和收率均随Brönsted酸浓度增加而逐渐升高, 考虑到Lewis酸浓度并未变化, 可知Brönsted酸是羟醛缩合反应性能的活性位点, 其浓度增加有利于羟醛缩合反应性能的提高. 同时, 对比不同ZSM-35分子筛失活现象, 高Brönsted酸浓度时分子筛重积炭量最高, 这可能是由于Brönsted催化不饱和产物关环生成芳烃物种或(和)发生氢转移过程所导致.

关键词: 羟醛缩合反应; 乙酸甲酯; HZSM-35分子筛; 酸性位; 丙烯酸

收稿日期: 2018-06-21. 接受日期: 2018-07-16. 出版日期: 2018-11-05.

*通讯联系人. 电话: (0411)84379998; 传真: (0411)84379038; 电子信箱: liuzm@dicp.ac.cn

#通讯联系人. 电话: (0411)84379418; 传真: (0411)84379038; 电子信箱: wlzhu@dicp.ac.cn

本文的电子版全文由Elsevier出版社在ScienceDirect上出版(http://www.sciencedirect.com/science/journal/18722067).